Journal of Power Sources 183 (2008) 557–563

Contents lists available at ScienceDirect

Journal of Power Sources

journal homepage: www.elsevier.com/locate/jpowsour

Non-platinum cathode catalyst layer composition for single Membrane Electrode Assembly Proton Exchange Membrane Fuel Cell

Tim S. Olson, Kate Chapman, Plamen Atanassov *

Chemical & Nuclear Engineering Department, University of New Mexico, Albuquerque, NM 87131, United States

ARTICLE INFO

Article history:
Received 7 April 2008
Received in revised form 3 May 2008
Accepted 6 May 2008
Available online 14 May 2008

Keywords:
Non-platinum electrocatalyst
Oxygen reduction
PEM fuel cell
Membrane electrode assembly
Catalyst layer

ABSTRACT

The performance of nano-structured templated non-platinum-based cathode electrocatalysts for proton exchange membrane fuel cells (PEMFC) was evaluated for different catalyst layer compositions. The effect of non-platinum catalyst, Nafion, and 35 wt% Teflon modified Vulcan XC-72 Carbon Blacks (XC-35) loadings were measured under H_2/air and H_2/O_2 conditions. Transport hindrances that occur in the catalyst layers are evaluated with ΔE vs. i analysis. It is shown that transport limitations in the cathode catalyst layer can limit the performance of the cell at relatively low current densities if the catalyst layer composition is not optimized. Further, a procedure is outlined here to aid in the implementation of non-traditional catalyst materials into fuel cell systems (i.e. templated electrocatalyst as compared to the standard supported material).

1. Introduction

State of the art proton exchange membrane fuel cells (PEMFC) and direct methanol fuel cells (DMFC) currently employ platinum-based catalysts at the anode and cathode. If fuel cell technology is to become competitive with other energy conversion technologies the overall materials cost is going to have to be reduced significantly. For example, Gasteiger et al. reported in 2004 that approximately a fivefold decrease in the platinum loading in the state of the art PEMFC stack is needed for mass commercialization of fuel cell powered automobiles [1]. One method to decrease the cost of the materials in the catalytic layers of a membrane electrode assembly (MEA) is to engineer catalysts with ultra-low precious metal loadings that still meet performance specifications. Researchers are currently engineering nano-structured supports, such as carbon nano-tubes to increase the dispersion of the precious metal catalyst and enhance transport in the active layer [2]. Others are attempting to decrease the platinum loading by creating core–shell particles that utilize a non-precious metal in the core and a thin platinum outer shell [3]. Alternatively, a less active but inexpensive catalyst could be used in larger quantities to meet the same power demands.

Non-platinum-based catalysts such as pyrolyzed macrocycles offer this alternative. The use of macrocycles as electrocatalysts has been studied for their unique catalytic properties since the 1960s [4]. An overwhelming amount of these reports have focused either on the effect of pyrolysis temperature, the metal center and/or ligand on the catalytic activity as determined by rotating disk electrode, rotating ring-disk electrode, or gas diffusion electrode/liquid electrolyte type analysis. Oxygen reduction reaction mechanistic studies in the literature have yielded a number of possible active moieties, including Me–N_x centers, graphitized carbon, and transition metal particles. While the activity of the graphitic phases and transition metal particles is debated in the literature, there is a general consensus that the central transition metal atom (i.e. Co, Fe, Ni, Mn, etc.) bonded to nitrogen in at least one coordination plays a role in the electrochemical reduction of oxygen [5–12]. More recently there have been a number of publications presenting MEA performance data using a non-platinum-based cathode catalyst [12–16]. It was shown that an iron-based catalyst had very similar performance to a MEA cathode consisting of 7.3 mg of a 2 wt% platinum E-TEC catalyst in a 1 cm^2 MEA [17]. There have been no studies evaluating the effect of the component loadings in non-platinum-based PEMFC cathodes or on alternative MEA fabrication procedures. If non-platinum catalysts are to be commercialized for use in PEMFC, significantly more work is going to have to be done in terms of engineering nano-structured materials and material implementation in realistic fuel cell systems.

The engineering of a non-platinum-based catalyst is considerably different from that of platinum and precious metal-based catalysts. Instead of increasing the precious metal utilization by

* Corresponding author. Tel.: +1 505 277 2640; fax: +1 505 277 5433.
E-mail address: plamen@unm.edu (P. Atanassov).

0378-7753/$ – see front matter © 2008 Elsevier B.V. All rights reserved.
doi:10.1016/j.jpowsour.2008.05.016

achieving ultra-low metal loadings the engineering task is to maximize the loading of the non-platinum catalyst. Gasteiger et al. at GM have suggested that if the catalyst is truly "costless" the performance of non-platinum catalysts can be more accurately compared in volumetric currents ($A\,cm^{-3}$), where the volume is determined by MEA geometric area and the thickness of the catalysis layer [1]. Therefore, a well-engineered non-platinum-based catalyst should not only be catalytically active for the reduction of oxygen but also promote reactant transport through a thick catalyst layer of a MEA.

Traditional electrocatalysts, including the state of the art precious metal-based and other non-platinum catalysts in the literature consist of a high surface area carbon black as a support to a decorating metal nano-particle phase or other active moieties (i.e. $Me–N_x$). The non-platinum catalysts that we have developed are not supported, instead they are templated on amorphous Cabosil® silica, pyrolyzed, and the silica template is removed. The end product is a porous and self-supported structure of only catalytic material. Here the performance of a cobalt-based oxygen reduction catalyst (CoTMPP) is evaluated in a PEMFC MEA environment. The effect of the cathode catalyst layer composition is measured and ΔE vs. i analysis is preformed to assess the transport hindrances that occur in the catalyst layer.

2. Experimental

2.1. Non-platinum catalysts synthesis

0.5 g of 5, 10, 15, 20-tetrakis(4-methoxy-phenyl)-porphine cobalt(II) was mixed with 100 ml of THF and 0.5 g of amorphous fumed Cabosil silica. The solvent was allowed to evaporate overnight and the templated material was collected and pyrolyzed under nitrogen flow at 700 °C for 4 h and quenched cooled. The silica template was then removed with a concentrated solution of KOH, washed, and allowed to dry.

2.2. Non-platinum 5 cm^2 MEA fabrication

The standard anode ink was prepared as follows: 40 mg of PtRu black, 500 mg DI H_2O, and 166 mg of 5% Nafion solution was sonicated and hand painted on an 1135 Nafion membrane.

The non-platinum cathode inks were prepared as follows: 2, 4, and 6 $mg\,cm^{-2}_{geometric}$ CoTMPP catalyst was mixed with various amounts of a 35 wt% Teflon/Vulcan XC-72 (noted here as XC-35) material ranging from 10% to 50% of the catalyst loading and 0.5:1 to 3:1 Nafion:catalyst weight ratio. The non-platinum cathode ink was then hand painted on an 1135 Nafion membrane (Ion Power) and the microporous layer of the gas diffusion layer (GDL LT 1400-W Low temperature, ELAT(R) GDL microporous layer on woven web) in a ratio of 1:9, respectively. The MEA was then pressed at 345 $N\,cm^{-2}$ at 125 °C for 10 min.

2.3. Non-platinum MEA testing

The MEA was placed in a 5 cm^2 cell with serpentine flow channels and the bolts were compressed to 80 in. lb. The fuel cell technologies fuel cell test station was used to obtain H_2/O_2 and H_2/air polarization curves. Polarization curves were obtained galvanostatically with a 30 s delay before data actuation. The anode and cathode gases were heated and humidified at 85 °C, and the flow rates were 266 and 466 sccm, respectively. The cell operating temperature was maintained at 80 °C. Polarization curves were acquired at 0 and 20 $N\,cm^{-2}$ backpressure.

3. Results

3.1. Non-full-factorial approach to MEA catalyst layer composition

Evaluating and optimizing the performance of non-platinum ORR electrocatalysts under realistic working fuel cell conditions is essential in catalyst selection and development. The cathode catalytic layer in the MEA consists of non-platinum catalyst, XC-35, and Nafion. For high performance the three-phase interface (catalyst, electrolyte, and reactant) must be well-dispersed through out the active layer.

In order to investigate the effect of the composition of the non-platinum MEA cathode catalyst layer and limit the amount of MEAs that were fabricated and tested, a non-full-factorial approach was used. This method can greatly reduce the number of combinations of component loadings that need to be tested to obtain a catalyst layer composition that is close to optimal. For example, a full-factorial design of experiments consisting of three components at three different loadings each results in 27 possible combinations. The technique used here can reduce the number of combinations to as few as 7 for the same 3 by 3 matrix. This is done by optimizing one parameter loading at a time using an iterative method if needed. For example, first select the three parameter loadings which are believed to be optimal or close to optimal. Then each parameter loading is varied by testing the performance at loading values above and below the optimal value. This process is continued for the other two parameters. Iteration is needed if the initial parameter loading value is found not to produce the best performance. This protocol is used to determine the catalyst loading for the templated non-platinum cathode catalyst, 35 wt% Teflon Vulcan/XC-72 carbon black material (XC-35), and Nafion content in the active layer.

All non-platinum cathode catalyst inks were hand painted onto the Nafion membrane and the microporous layer of the GDL in a ratio of 1:9, respectively. The ink was applied in this fashion to utilize the porous structure of the templated non-platinum catalyst. The resulting thickness of the cathode catalyst layers evaluated in this study did not change appreciably. For this reason the performance of the non-platinum catalyst is not reported in $A\,cm^{-3}$ as was suggested by Gasteiger et al. [1], but in the standard $A\,cm^{-2}$ which is normalized by the geometric area of the MEA. Fig. 1 shows TEM (a) and SEM (b) micrographs of CoTMPP after pyrolyzation at 700 °C and removal of the silica template. The TEM image shows two distinct cobalt phases on the surface of the porous catalyst. The first being a nano-particle phase and the second being a dendrite-like phase. The porous structure of the templated catalyst as well as the dendrite-like structures on the surface that form during pyrolysis can be seen in the SEM micrograph.

3.2. Non-platinum cathode MEA composition and performance

The effect of MEA cathode composition on performance was evaluated in a fuel cell test station under H_2/O_2 and H_2/air conditions. Initially an MEA was fabricated with what was believed to be the optimal catalyst layer composition of 4 $mg\,cm^{-2}$ catalyst, XC-35 loading of 40 wt% to catalysts loading (1.6 $mg\,cm^{-2}$), and a 1:1 Nafion to catalyst weight ratio. Variations of this composition were then fabricated and tested following the non-full-factorial approach outlined above.

The catalyst loading was varied at 2, 4, and 6 $mg\,cm^{-2}$ while the XC-35 and Nafion content was held constant at 40 wt% and 1:1 wt ratio, respectively. Fig. 2 shows that peak performance is obtained with 4 $mg\,cm^{-2}$ CoTMPP catalyst loading. The XC-35 loading was then optimized while holding the catalyst loading

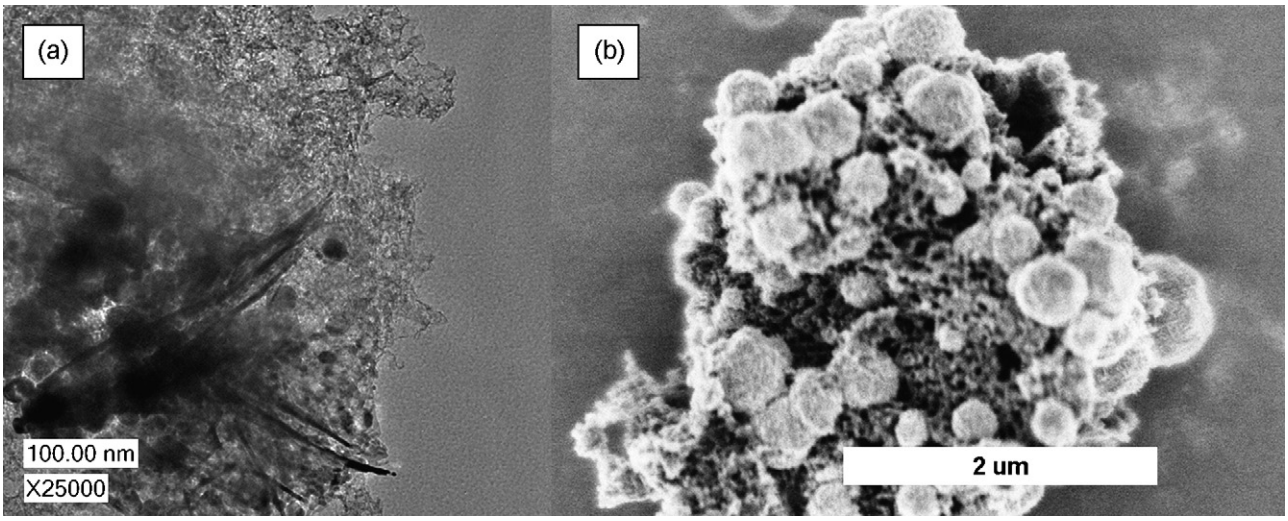

Fig. 1. TEM (a) and SEM (b) micrographs of CoTMPP that has been templated on Cabosil silica, pyrolyzed at 700 °C, and treated with KOH to remove the silica template.

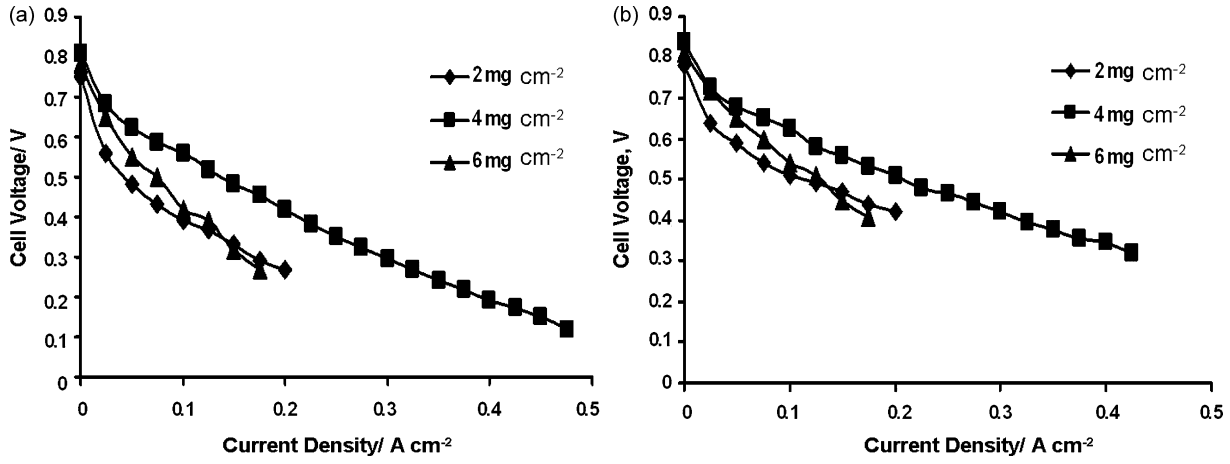

Fig. 2. Polarization curves showing the effect of non-platinum catalyst loading (2, 4, 6 mg $cm^{-2}_{geometric}$) in the cathode while holding XC-35 (40 wt% of catalyst weight) and Nafion loading constant (1:1 weight ratio of Nafion:catalyst). The curves were obtained with inlet gases heated and humidified to 85 °C, zero back pressure and the cell temperature was held at 80 °C in (a) H_2/air and (b) H_2/O_2.

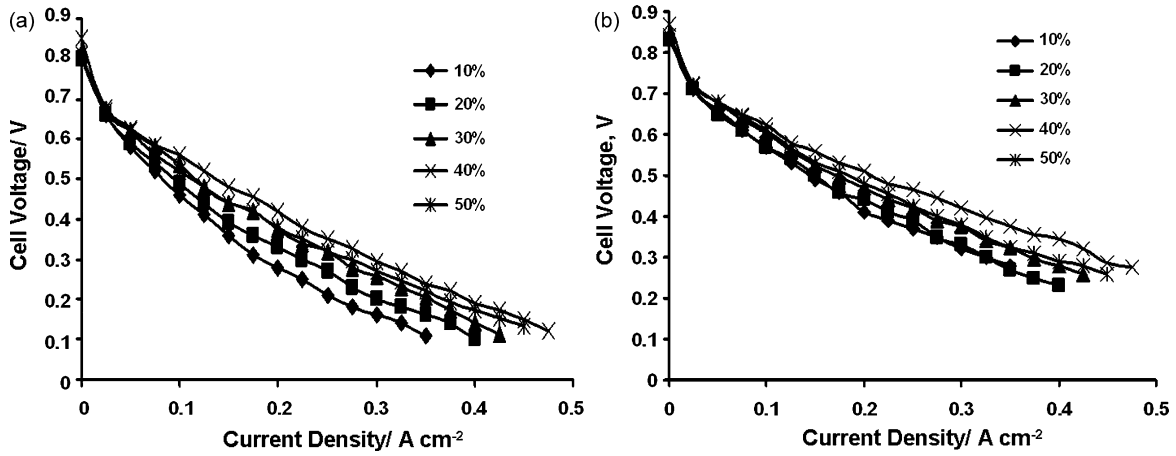

Fig. 3. Polarization curves showing the effect of XC-35 loading (10%, 20%, 30%, 40%, 50% by weight of the non-platinum catalyst loading) in the cathode while holding non-platinum catalyst (4 mg cm^{-2}) and Nafion loading constant (1:1 weight ratio of Nafion:catalyst). The curves were obtained with inlet gases heated and humidified to 85 °C, 0 back pressure and the cell temperature was held at 80 °C in (a) H_2/air and (b) H_2/O_2.

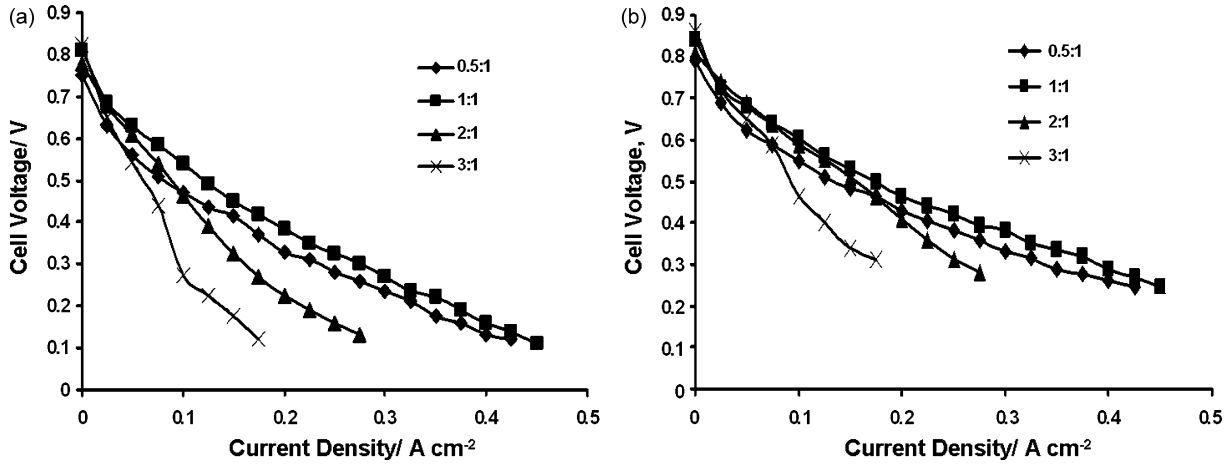

Fig. 4. Polarization curves showing the effect of Nafion loading (0.5:1, 1:1, 2:1, 3:1 weight ratio of Nafion:catalyst) in the cathode while holding XC-35 (40 wt% of catalyst weight) and non-platinum catalyst (4 mg cm^{-2}). The curves were obtained with inlet gases heated and humidified to 85 °C, 0 back pressure, and the cell temperature was held at 80 °C in (a) H_2/air and (b) H_2/O_2.

and Nafion content constant at 4 mg cm^{-2} and 1:1 weight ratio, respectively. Fig. 3 indicates that 40 wt% of the catalyst loading is most favorable. Finally, the Nafion to catalyst weight ratio was optimized. Fig. 4 shows that the 1:1 weight ratio has the best performance.

3.3. Determination of overpotential terms in non-platinum-based cathode MEA

In order to determine which aspects of non-platinum oxygen reduction catalysis need to be focused on it is important to identify the individual contributions of the overpotential terms. Eq. (1) describes the cell voltage, E_{cell} in terms of the highest obtainable theoretical voltage and common inefficiencies that limit the overall fuel cell performance. Where E_{rev} is the thermodynamically determined reversible H_2/O_2 cell voltage, which is a function of the reactant partial pressures and temperature, η_{ohmic} is the ohmic or iR overpotential, η_{ORR} is the oxygen reduction kinetic overpotential, and η_{tx} is the mass transport overpotential.

$$E_{cell} = E_{rev}(p_{H_2},\ p_{O_2},\ T) - \eta_{ohmic} - \eta_{ORR} - \eta_{tx} \quad (1)$$

The ohmic overpotential, η_{ohmic} can be determined by multiplying the high-frequency resistance of the cell by the current density. High-frequency resistance measurements yielded similar values for all the non-platinum-based cathode MEA layer compositions. The high-frequency resistance values were all in the range of $0.4 \pm 0.05\ \Omega\ cm^2$. These values are an order of magnitude higher than what is typically reported for a cell operating with a standard Pt supported on carbon cathode catalyst [1]. This can possibly be attributed to the overall lower intrinsic conductivity of the templated non-platinum material.

The specific contribution from the oxygen reduction kinetic overpotential, η_{ORR} was estimated by performing Tafel analysis on iR-corrected polarization curves obtained in oxygen and air. Fig. 4 shows Tafel-type plots for the non-platinum cathode MEA catalyst layer composition that resulted in the best performance as determined in Section 3.2. Within the Tafel region (i.e. low current densities <0.1 A cm^{-2}) Tafel slopes of 120 and 150 mV dec^{-1} were obtained during cell operation in oxygen and air, respectively. If it is assumed that the effect of hydrogen crossover is minimal and the oxygen reduction overpotential term for a non-platinum-based cathode MEA follows the same Tafel-type dependence at all measured current densities then its individual contribution can be estimated. This is done by extrapolation of the Tafel slope obtained at low current densities over the desired current regime. A plot of this nature shows the theoretical performance of a cell operating without ohmic and transport overpotentials (i.e. $\eta_{ohmic} = \eta_{tx} = 0$). Further, the individual contribution of the transport overpotential can be assessed by adding the experimentally determined ohmic losses to the purely kinetically controlled curve. This analysis was preformed for the polarization curve obtained under air feed to the non-platinum-based cathode. Fig. 5 shows the experimental obtained E_{cell} curve, E_{cell} free of η_{tx}, and E_{cell} free of η_{tx} and η_{ohmic}. It is seen that the kinetic oxygen reduction overpotential is responsible for a majority of the losses in the cell. For example, at a current density of 0.2 A cm^{-2} the approximant individual overpotential contributions to be 450 mV for η_{ORR}, 80 mV for η_{ohmic}, and 150 mV for η_{tx} (Fig. 6).

Based solely on this analysis the future development and success of non-platinum oxygen reduction catalysis would rely on substantially decreasing the kinetic oxygen reduction overpotential. This can be achieved by engineering non-platinum-based catalysts that largely support either the direct four electron reduction pathway or the 2×2 electron series pathway where oxygen is first reduced to peroxide and peroxide is further reduced to water. If one was to approach the development of non-platinum catalysts in this way, fundamental oxygen reduction mechanistic studies would be

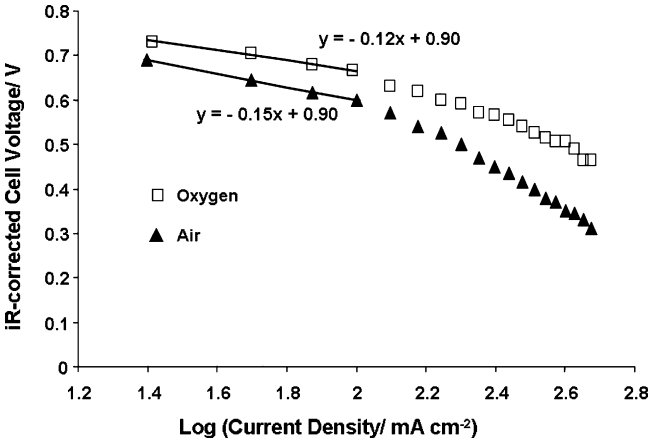

Fig. 5. Tafel plots for the best performing non-platinum cathode MEA composition obtained in H_2/air and H_2/O_2 with inlet gases heated and humidified to 85 °C, 0 back pressure, and cell temperature of 80 °C.

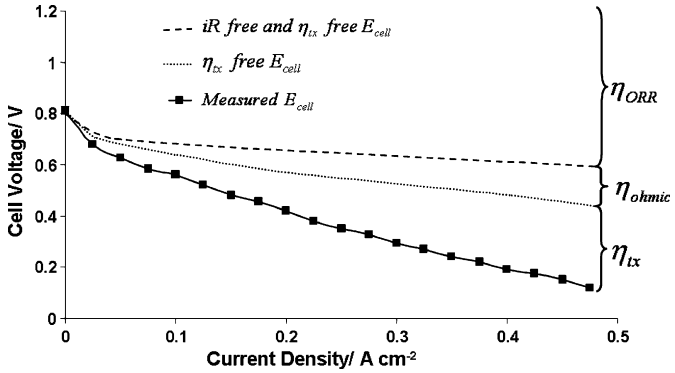

Fig. 6. Polarization curve for the best performing non-platinum cathode MEA composition obtained in H_2/air with inlet gases heated and humidified to 85 °C, 0 back pressure, and cell temperature of 80 °C. Theoretical polarization curves are also included showing the effect of ohmic and transport overpotentials.

needed to identify moieties with the highest activity for the desired reaction pathways.

A more realistic comparison of the individual overpotentials contributions in terms of realistic obtainable performance can be made by evaluating non-platinum oxygen reduction catalysts with respect to the state-of-the-art platinum-based catalysts. For example, similar analysis was preformed to elucidate the individual overpotential contributions for a H_2/O_2 fuel cell operating with a platinum-based cathode catalyst [1]. If the ohmic and transport free overpotential polarization curves for the non-platinum (shown here) and platinum [1] based MEA cathodes are compared more realistic performance benchmarks can be established for non-platinum catalysts. At 0.2 A cm^{-2} there is approximately 140 mV difference in the ohmic and transport free overpotential curves for the platinum and non-platinum-based cathodes. Currently, it is unreasonable to think that non-platinum catalysts will be able to match the performance of platinum-based catalysts in the near future. Therefore a more reasonable goal would be to decrease the difference in the purely kinetic overpotential curves by a factor of 2. In order to achieve this increase in efficiency the kinetic overpotential at 0.2 A cm^{-2} would need to be decreased by 70 mV.

From this reasoning a practical reduction in the current inefficiencies that occur in non-platinum-based MEA cathodes can be made by targeting any or all of the overpotential terms given in Eq. (1). The following section will provide further insight on transport hindrances that occur within the non-platinum MEA cathode catalyst layer.

3.4. Analysis of transport hindrances in non-platinum MEA catalyst layer

Further information on the limiting processes that occur in the catalyst layer during fuel cell operation can be exemplified with ΔE vs. i analysis. ΔE vs. i analysis is used to elucidate the transport hindrances that occur in the active layer that strongly influence the overall performance of the electrode. The analysis is done by first obtaining polarization curves in oxygen and air. Next, the difference of the potentials of the electrode while operating in oxygen and air at the same current density is taken. This difference in potentials is theoretically described by the following equation [18]:

$$\Delta E = E_{O_2}(i) - E_{air}(i) = \frac{RT}{\alpha nF}\ln\left(\frac{P_{O_2}}{P_{air}}\right) + \frac{RT}{\alpha nF}\ln\left(\frac{f_{O_2}(i)}{f_{air}(i)}\right) \quad (2)$$

The first term is independent of current and shows the oxygen partial pressure dependence. The second term incorporates the dependence on current density with the efficiency factors for

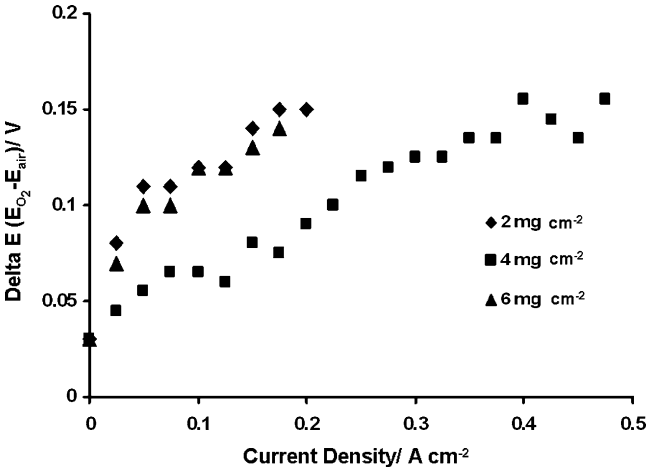

Fig. 7. ΔE vs. i curves obtained from the H_2/air and H_2/O_2 polarization curves showing the effect of non-platinum catalyst loading in Fig. 2.

oxygen f_{O_2} and air f_{air}. The efficiency factors are similar to effectiveness factor in that it is defined as the ratio of currents at a given potential for the real electrode and a hypothetical electrode with the same surface area and no transport losses. At high current densities the second term begins to increase because the efficiency of the electrode operated under air will decrease more rapidly than when under oxygen operation. For example, an electrode that operates relatively free of transport hindrances would produce a ΔE vs. i curve with a small slope (i.e. flat line). While an electrode with severe transport hindrances would result in a curve with a steep slope. This technique is used here to evaluate the transport processes that occur in the MEA cathode catalyst layers that were shown in Section 3.2.

Fig. 7 illustrates the ΔE vs. i behavior for the 3 CoTMPP catalyst loadings of 2, 4, and 6 mg cm^{-2} (Fig. 2). The analysis indicates that the intermediate loading of 4 mg cm^{-2} produced the catalyst layer with least amount of transport hindrances. We can speculate that the lower catalyst loading of 2 mg cm^{-2} had insufficient active sites to maintain higher current densities. While the higher loading of 6 mg cm^{-2} could have possibly clogged the gas transport regions of the GDL or produced a catalyst layer that is too thick.

ΔE vs. i curves for XC-35 loadings (Fig. 3) are found in Fig. 8. The analysis indicates that increasing the XC-35 loading to approximately 40 wt% of catalyst loading can reduce the transport hindrances that occur in the catalyst layer. This result indicates

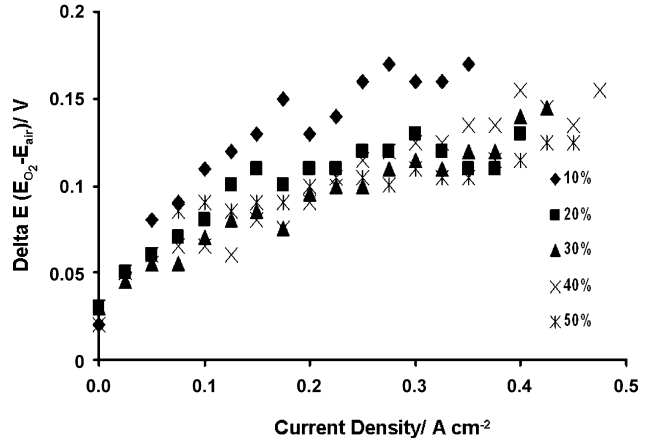

Fig. 8. ΔE vs. i curves obtained from the H_2/air and H_2/O_2 polarization curves showing the effect of XC-35 loading in Fig. 3.

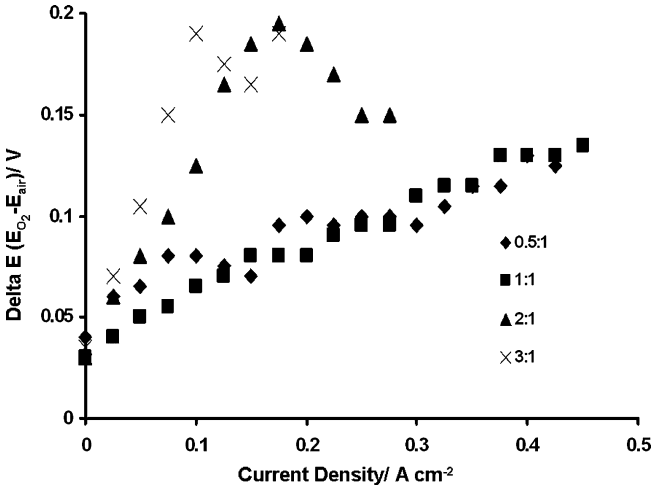

Fig. 9. ΔE vs. i curves obtained from the H_2/air and H_2/O_2 polarization curves showing the effect of Nafion loading in Fig. 4.

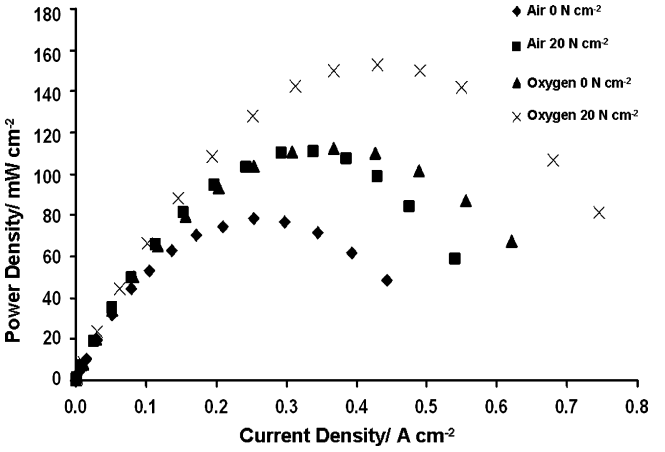

Fig. 10. Power curves and polarization curves for the best performing non-platinum cathode composition (4 mg cm^{-2} non-platinum catalyst, 40 wt% XC-35, and 1:1 weight ratio Nafion:catalyst). The curves were obtained with inlet gases heated and humidified to 85 °C, 0 and 20 N cm^{-2} back pressure, and the cell temperature was held at 80 °C in H_2/air and H_2/O_2.

the need for a dispersed hydrophobic phase in the catalyst layer. The addition of the XC-35 is needed to promote oxygen transport into the layer and the removal of product water that is formed within the layer. It is possible that the dispersed hydrophobic phase could also minimize phase segregation of the non-platinum catalyst layer components and effectively increase the amount of accessible three-phase boundary active sites. For example, phase segregation of the non-platinum catalyst material and Nafion will occur in the catalyst layer due to the hydrophilic nature of the non-platinum catalyst and the hydrophobic properties of the highly fluorinated Nafion polymer. Addition of XC-35 (which consists of carbon black (Vulcan XC-72) and Teflon) to the non-platinum catalyst layer will promote contact and interaction of the components.

Fig. 9 shows ΔE vs. i analysis for electrodes prepared with different Nafion to catalysts ratios (Fig. 4). It can be observed that increased Nafion content (3:1 and 2:1) produces significant transport hindrances. While the 1:1 and 0.5:1 ratios show less significant transport hindrances. This result can be contributed to the thickness of the Nafion film covering the catalyst material. High active site density is achieved by engineering a well-dispersed and highly accessible layer of sites that promote the necessary three phase boundary. Here it is suggested that the 1:1 Nafion:catalyst weight ratio produced the catalyst layer with the highest density of accessible sites without severe transport limitations. At higher Nafion loadings the Nafion film became too thick and diffusion of the reactive species through that film becomes limiting. It has been established that catalyst layers fabricated with a standard electrocatalyst (i.e. platinum nano-particles supported on a high surface area carbon black) provided the highest performance with approximately 20 wt% Nafion content. This standard catalyst layer composition translates to approximately a 1:1 catalyst material to Nafion volume ratio. From the PEMFC data and ΔE vs. i analysis shown here it is evident that implementation of new materials into fuel cell systems is not straight forward. For this reason it is important to develop procedures, like the one outlined here that can limit the time and resources needed to obtain the proper catalyst layer composition.

Comparison of the two analysis techniques used here to elucidate inefficiencies due to transport limitations yield somewhat different results. The ΔE values obtained in the ΔE vs. i analysis of the non-platinum MEA cathodes are lower than the magnitude of the transport overpotential term as determined in Section 3.3. This discrepancy can be explained by the fact that the ΔE vs. i analysis shows only the effect of the concentration overpotential on electrode performance. Other limiting processes that are occurring in the electrode and are not influenced by changing the reactant partial pressure are not accounted for. For example, H_2 crossover was not accounted for in the analysis. It is very likely that the larger transport overpotential term as determined in Section 3.3 is a result of the unaccounted H_2 crossover.

3.5. Non-platinum H_2/air–O_2 power curves

Fig. 10 shows the attainable power densities for the highest performing non-platinum catalyst MEA composition. The curves shown are for H_2/air and H_2/O_2 at 0 and 20 N cm^{-2} backpressure and 80 °C. The peak power density obtained under non-pressurized H_2/air feed was found to be approximately 80 mW cm^{-2} at 0.25 A cm^{-2}. Under pressurized H_2/O_2 operating conditions the peak power density increases about 150 mW cm^{-2} at 0.45 A cm^{-2}.

4. Conclusions

The H_2/air–O_2 MEA performance was evaluated for different catalyst layer compositions utilizing a templated non-platinum ORR catalyst. A non-full-factorial approach was used to limit the number of compositions fabricated and tested and still obtain high performance data. Further ΔE vs. i analysis was used to elucidate the transport hindrances that occur in the MEA catalyst layer. From this analysis it is evident that transport processes are limiting the overall performance even at relatively low current densities.

If non-platinum catalysts are to be commercialized, significantly more work is needed. Specifically, the performance of more non-platinum catalysts needs to be recorded in MEA environments. This includes other catalysts (i.e. supported and templated) as well as MEA catalyst layer formulations. These undertakings should focus on increasing the overall site density in the MEA catalyst layer. One of the more likely possible applications of non-platinum ORR electrocatalysts will be in DMFC due to the methanol tolerance. This study provides a method to optimize the cathode catalyst layer not only in hydrogen fuel cells but also in methanol based fuel cells.

References

[1] H. Gasteiger, S. Kocha, B. Sompalli, Appl. Catal. B 56 (2005) 9–35.
[2] J.M. Tang, K. Jansen, M. Waje, W. Li, P. Larsen, K. Pauley, Z. Chen, P. Ramesh, M.E. Itkis, Y. Yan, RC, J. Phys. Chem. C 111 (2007) 17901–17904.

[3] K. Sasaki, R.R. Adzic, J. Electrochem. Soc. 155 (2008) B180–B186.
[4] R. Jasinski, J. Electrochem. Soc. 112 (1965) 526–528.
[5] K. Wiesener, Mater. Chem. Phys. 22 (1989) 457–475.
[6] M.C.M. Alves, J.P. Dodelet, D. Guay, M. Ladouceur, G. Tourillon, J. Phys. Chem. 96 (1992) 10898–10905.
[7] J. Zagal, M. Paez, A.A. Tanaka, J.R. Dossantos, C.A. Linkous, J. Electroanal. Chem. 339 (1992) 13–30.
[8] G. Faubert, G. Lalande, R. Cote, D. Guay, J.P. Dodelet, L.T. Weng, P. Bertrand, G. Denes, Electrochim. Acta 41 (1996) 1689–1701.
[9] M. Lefevre, J.P. Dodelet, Electrochim. Acta 48 (2003) 2749–2760.
[10] H. Schulenburg, S. Stankov, V. Schunemann, J. Radnik, I. Dorbandt, S. Fiechter, P. Bogdanoff, H. Tributsch, J. Phys. Chem. B 107 (2003) 9034–9041.
[11] S. Marcotte, D. Villers, N. Guillet, L. Roue, J.P. Dodelet, Electrochim. Acta 50 (2004) 179–188.
[12] F. Jaouen, J.P. Dodelet, Electrochim. Acta 52 (2007) 5975–5984.
[13] F. Jaouen, S. Marcotte, J.P. Dodelet, G. Lindbergh, J. Phys. Chem. B 107 (2003) 1376–1386.
[14] F. Jaouen, F. Charreteur, J.P. Dodelet, J. Electrochem. Soc. 153 (2006) A689–A698.
[15] C. Medard, M. Lefevre, J.P. Dodelet, F. Jaouen, G. Lindbergh, Electrochim. Acta 51 (2006) 3202–3213.
[16] Z. Ma, X. Xie, X. Ma, D. Zhang, Q. Ren, N. Heb-Mohr, V. Schmidt, Electrochem. Commun. 8 (2006) 389–394.
[17] G. Faubert, R. Cote, J.P. Dodelet, M. Lefevre, P. Bertrand, Electrochim. Acta 44 (1999) 2589–2603.
[18] A. Kaisheva, I. Iliev, S. Gamburzev, J. Power Sources 13 (1984) 181–195.